Journal of Al-Azhar University Engineering Sector

Vol. 14, No. 53, October, 2019, 1424-1435

FLEXURAL BEHAVIOR OF PRESTRESSED CONCRETE BEAMS STRENGTHENED BY NEAR SURFACE MOUNTED FRP RODS

***Belal Hesham Elharouney[1] Ayman Hussein[2], Ezz El-Deen Mostafa[2] and Amr Elnemr[3]**

[1] Structural design engineer at ASGC, Misr algadida, Cairo, Egypt

[2]Structural Engineering Department, Faculty of Eng., Ain Shams University, Cairo, Egypt

[3]Structural Engineering Department, German University, Cairo, Egypt

*Orresponding author E-mail: Belalelharouney@gmail.com

ABSTRACT

The applications of post tensioned concrete have increased and have now been used in different regions of the world. There are only few studies which have studied the behavior of retrofitted prestressed concrete experimentally, with the major part of the studies focusing on retrofitted reinforced concrete. This research study is initiated by a desire to more fully investigate the response of it. This paper presents a parametric study established on a beam with T-sec with web width 700 mm and a height of 1800mm, the thickness of the flange is 150 mm, the width of beam flange is 1500mm with span 29.6m. The beam was simply supported and loaded uniformly. A total no. of 20 finite element 3D models was generated taking the all possible failure modes such as FRP rupture, concrete cover separation and concrete crushing in order to study percentage of prestressing steel (Wp) parameter. Finally, a comparison is done between ACI 440.2R-08 code and the finite element results for the ultimate failure load and the predicted failure mode 0

Key Words: Posttensioned beam, FRP, NSM, Reinforced concrete beams, Strengthening

سلوك الكمرات الخرسانية سابقة الإجهاد المدعمة بالقضبان البوليمرية المسلحة بالألياف المدفونة بالقرب من السطح تحت تأثير عزم الانحناء

بلال هشام الحاروني[١] و أيمن حسين حسني خليل [٢] عز الدين مصطفي [٢] و عمرو ماهر النمر [٣]

[١] شركة الشعفار للمقاولات.- مصر الجديدة - القاهرة- جمهورية مصر العربية

[٢] قسم الهندسة المدنية - ،كلية الهندسة ، جامعة عين شمس ،القاهرة، مصر

[٣] قسم الهندسة الإنشائية ، كلية الهندسة ،الجامعة الألمانية.- التجمع الخامس - القاهرة

ملخص البحث

تطبيقات الخرسانة سابقة الإجهاد أصبحت واسعة الانتشار في كل إنحاء العالم وخاصة في الكباري الخراسانية ذات البحور الطويلة في حدود ٣٠ إلي ٤٠ متر لذلك كان لابد من دراسة تدعيم او تقوية هذا النظام باستخدام الفيبر المسلح المدفون بالقرب من السطح.في الوقت الحالي كانت غالبية الدراسات تركز علي تدعيم الخرسانة المسلحة ويوجد حاليا دراسات بسيطة تطرقت الي هذا المجال عمليا فقط لذلك تركزت هذه الدراسة علي الناحية النظرية و التمثيل الدقيق لسلوك الكمرة المدعمة للحصول علي حمل الكسر وتحديد نوع الانهيار.

تم عمل دراسة نظرية علي كمرة بقطاع T-section جميع هذه الكمرات لها ارتفاع ثابت هو ١٨٠٠ مم وعرض جزع الكمرات٧٠٠مم وسمك الشفة العلوية (البلاطة) ١٥٠ مم و بعرض ثابت قدره ١٥٠٠ مم .وتم تدعيم هذه الكمرات بالقضبان البوليمارية المدفونة بالقرب من السطح بإعداد مختلفة وكانت الكمرة بسيطة الارتكاز محملة بحمل موزع.
حيت تم عمل 20 نموذج تحليلي باستخدام برنامج ال ABAQUS تدرس تأثير النسبة المئوية لكابلات سابقة الشد في القطاع.ولكي يتم تقييم النتائج النظرية تم عمل مقارنة حمل الانهيار ونوع الانهيار بين الكود الأمريكي ACI 440.2R-0.8

الكلمات المفتاحية: كمرة لاحقة الشد – الفيبر المسلح بالبوليمر-الالياف المدفونة بالقرب من السطح-كمر مسلح-التدعيم.

1. INTRODUCTION

In bridges, the main common elements are the prestressed beams because of large spans and heavy loads, the major benefit of these beams is that they have smaller depth than the traditional beams. In order to protect beam from cracks due to fatigue loads or due to the increasing of loads, strengthening might be done. By strengthening, the cracks are greatly reduced and the sizes and the widths are considerably reduced. There are several examples of strengthening methods. There are only few studies which have examined the behavior of retrofitted prestressed concrete experimentally, while the majority of the studies focusing on retrofitted reinforced concrete.

The scope of this paper can be summarized as follow:

a) Studying theoretically the ultimate flexural strength of posttension beam strengthened with NSM FRP

b) Evaluating the Finite element models results with the imperial formula by ACI 440.2R-08 code.

2. FINITE ELEMENT MODELLING

ABAQUS 2016 is used to simulate the finite element model. Due to the symmetry of the geometry, loadings and boundary conditions, only half of the beams is modeled using symmetry boundary conditions in one plane.

2.1 MATERIAL MODEL

2.1.1 UNIAXIAL BEHAVIOUR OF PLAIN CONCRETE

ABAQUS 2016 provides more than one model for the concrete. Concrete damage plasticity model is used to model the concrete beam in the present study. In this concrete damage plasticity model, the concrete dilation angle is taken as 50 for all beams. In addition, the other required parameters, namely, eccentricity, ratio of biaxial and uniaxial state strengths (fb0/fc0), ratio of the distance between the hydrostatic axis and deviatoric cross section (K), and viscosity parameter are taken as recommended in the ABAQUS manual (2010). The relation between σ_c and ε_c is shown in Figure (1) and was generated according to stress-strain relation for non-linear structural analysis (BS EN1992-1-1). The tension stiffening effect was considered by modifying the descending portion of stress-strain relations after cracking. The tension stiffening effect was assumed that the stress in tension droped to the residual stress at a strain of about ten times that at cracking. The relation between the stress and the cracking strain is shown in figure (2)

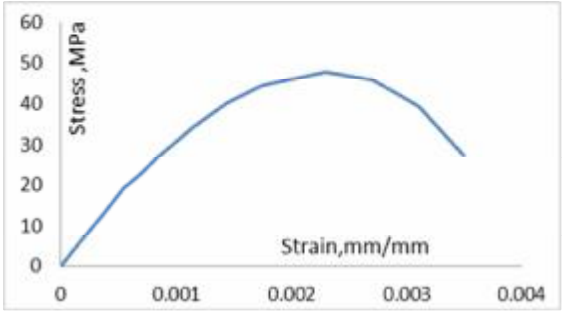

Figure (1) Compressive stress-strain curve

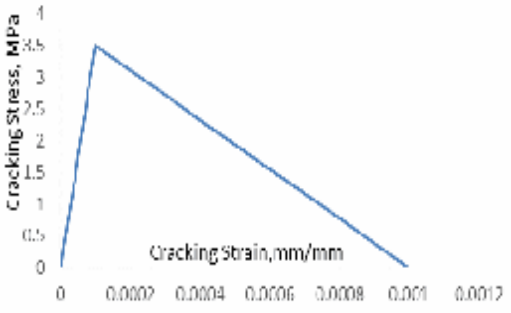

Figure (2) Tension Stress-Strain curve

2.1.2 UNIAXIAL BEHAVIOUR OF STEEL REINFORCEMENT

The values of (f_y) and (E_s) used to define the bilinear relationship for the non prestressing reinforcement were 420 MPa and 200100 MPa respectively as shown in Figure (3). The nonlinear stress-strain relationship for prestressing steel followed the empirical stress-strain model developed by Devalapura and Tadros (1992) for Grade 270 seven-wire strands as shown in Figure (4).

\

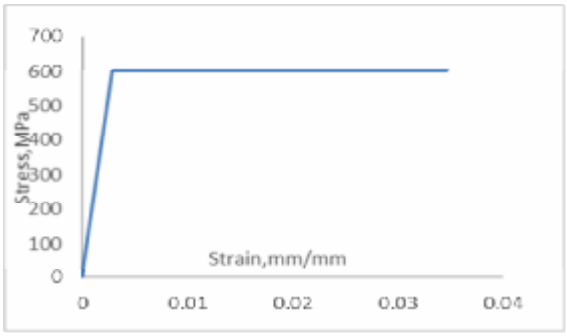

Figure (3) Tensile Stress–Strain Curve of non prestressed Steel Reinforcement

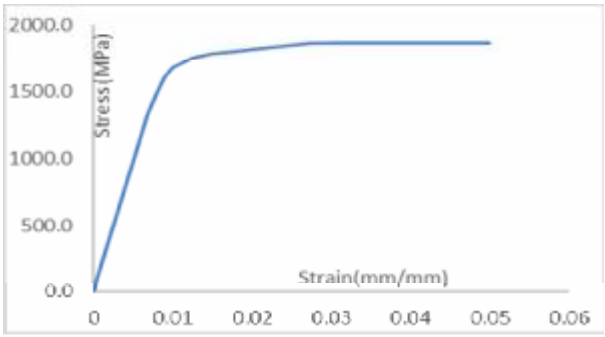

Figure (4) Tensile Stress–Strain Curve of prestressed Steel Reinforcement

2.1.3 UNIAXIAL BEHAVIOR OF FRP BARS

A perfect elastic stress strain curve is used to model the tensile behavior of the CFRP bars the tensile behavior was linear up to the ultimate tensile strength as represented in figure (5), after ultimate tensile strain(ε_{fu}) the tensile strength of CFRP bars effect is neglected.

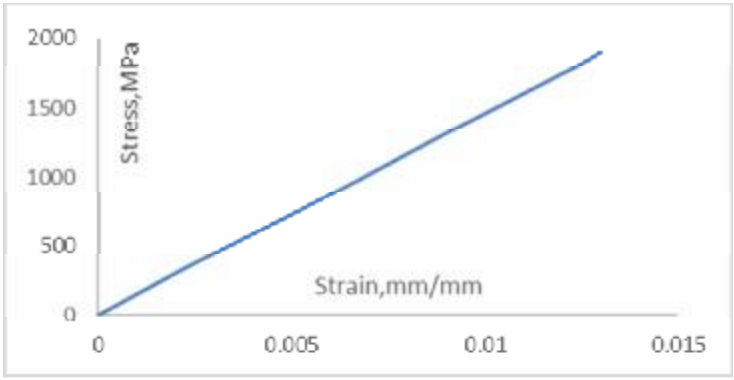

Figure (5) Tensile Stress–Strain Curve of FRP Bar

2.1.4 UNIAXIAL BEHAVIOR OF EPOXY ADHESIVE

The elasto-perfectly plastic stress strain diagram for modeling the tensile behavior of the epoxy as represented in figure (6).

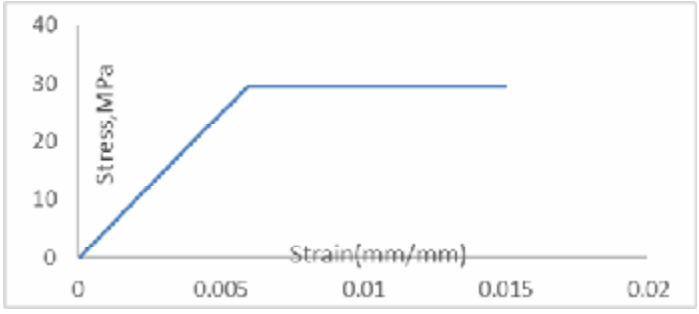

Figure (6) Tensile Stress–Strain Curve of Epoxy Adhesive

2.2 INTERACTION BETWEEN PARTS

The interaction between concrete beam and interior steel reinforcement was simulated using the embedded element constraint available in ABAQUS program that ensure that the bond between steel reinforcement and concrete was assumed as a perfect bond as presented in figure (7).

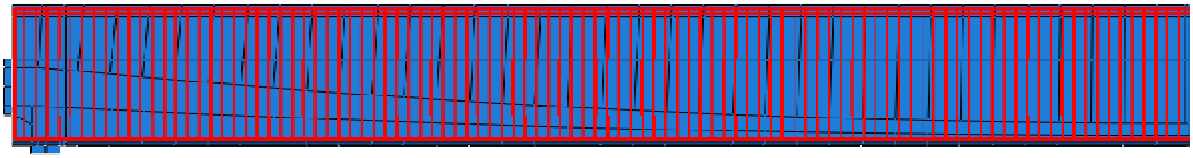

Figure (7) Host and embedded region(steel reinforcement in concrete beam)

The interaction between epoxy resin and FRP bars, FE model considered perfect bond between (epoxy-FRP) interfaces due to the fact that debonding failure was not observed in relevant tests. The interaction between the FRP bars and the epoxy resin was simulated using the embedded element constraint available in ABAQUS program. Figure (8) shows the host (purple) and embedded regions (red).

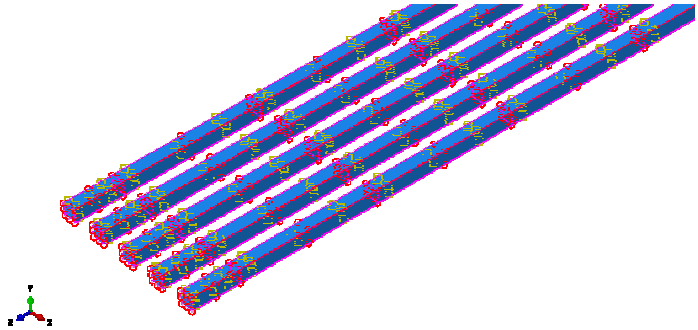

Figure (8) Host and embedded region (FRP embedded in epoxy Resin)

The Interaction between concrete beam and epoxy interfaces, surface-to-surface contact pairs were assigned to the concrete-epoxy interface with cohesive behavior using a cohesive zone model:

1) Normal Tension Stress-Gap Mode, The tensile resistance at the concrete-epoxy interface is assumed to be limited to the tensile capacity of the weakest material which is the concrete tensile strength presented in Equation (1) Therefore, the fracture energy of the interface under tensile stress is considered to be equal to the fracture energy of the concrete presented in Eq.(2) proposed by the CEB-FIP Model Code (1993) The contact gap Eq.(4) is derived using Equation (1) and Equation (2) to satisfy the tensile fracture energy based on the concrete tensile strength.

$$\sigma_{max} = 0.6\sqrt{f'_c} \quad \text{..... (1)}$$

$$G_{cn} = G_{fo}\left(\frac{f_c}{10}\right)^{0.7} \quad \text{..... (2)}$$

$$u_f = G_{fo}\left(\frac{\sqrt{10}\,f'_c}{24.3}\right)^{0.2} \quad \text{..... (3)}$$

u_f= contact gap at the completion of debonding (mm), and G_{fo}= the base value of fracture energy (N/mm), which depends on the maximum aggregate size. For concrete with maximum aggregate size of 20 mm, G_{fo} is calculated as 0.03475 N/mm by non-linear interpolation between different size values of aggregate as mentioned in the CEB-FIP Model Code (1993).

2) Shear Stress-Slip model, In the NSM FRP strengthened RC beam, the debonding occurs at the concrete epoxy interface which is the weakest interface and the identification of appropriate bond behavior that can be reasonably applicable to the NSM technique.The developed cohesive zone material model starts with an increasing segment up to the ultimate shear stress (τ_{max}) and its corresponding slip (δ_u) and then continues with a softening behavior up to the ultimate reached slip which was assumed to equal to four times the slip corresponding to the ultimate shear stress[5]. The value of τ_{max} for each

model is obtained using Eq. (4) which is suggested by Hassan and Rizkalla in case of round deformed bars [2]

$$\tau_{max(epoxy-concrete)} = \frac{f_{ct}\mu}{G_1} \quad \text{..... (4)}$$

A value of $\mu = 1$ is used as proposed by De Lorenzis and Teng [6]. G1 is a coefficient determined from the finite element analysis proposed by Hassan and Rizkalla based on a unit radial pressure applied at the bar location and using specified groove dimensions, concrete and adhesive properties, $G1$ is the taken equal to 0.65.

The initiation of damage was assumed to occur when a quadratic traction function involving the nominal stress ratios reached the value one. This criterion can be represented by:

$$\left\{\frac{\sigma_n}{\sigma^o_n}\right\}^2 + \left\{\frac{\sigma_s}{\sigma^o_s}\right\}^2 + \left\{\frac{\sigma_t}{\sigma^o_t}\right\}^2 = 1 \quad \text{..... (5)}$$

Where, σ^o_n, σ^o_s and σ^o_t represent the maximum values of the contact stress when the separation is normal to the interface or in the first or the second shear direction. The damage evolution law explains the rate of the cohesive stiffness degradation once the corresponding initiation criterion is reached Benzaggah–Kenane fracture criterion is used to define the damage evolution concept This criterion can be represented by:

$$G^n_s + (G^c_s - G^c_n)\left\{\frac{G_S}{G_T}\right\}^{\eta} = G^c \quad \text{.....(6)}$$

Where $G_S = G_{s+} G_t$ and $G_T = G_n + G_S$ where η is a cohesive property parameter, Where G_n, G_s and G_t refer to the work done by the traction and its conjugate separation in the normal, the first and the second shear directions, respectively. The values used for this study were G^n_s =0.048 N/mm, $G^c_t = G^c_s$=1.08 N/mm, and η=1 as shown in figure (9) which shows contact interfaces between epoxy and concrete.

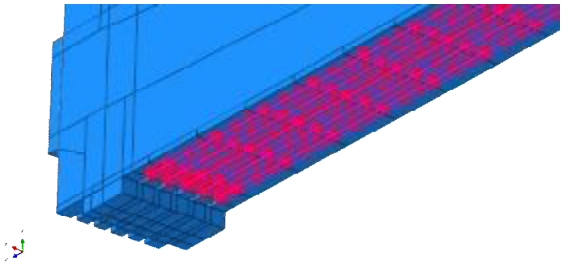

Figure (9) Cohesive Contact interfaces

Interaction between concrete beam and interior prestressing steel reinforcement is shown in figure (10), the grouting technique is simulated by changing the constitutive model for the tangential contact formulation from “frictionless” in the first step to infinitely “rough.” In the second step. A particular rigid beam MPC is a good choice to anchor the tendon end nodes to the anchor plate nodes as shown in figure (11)

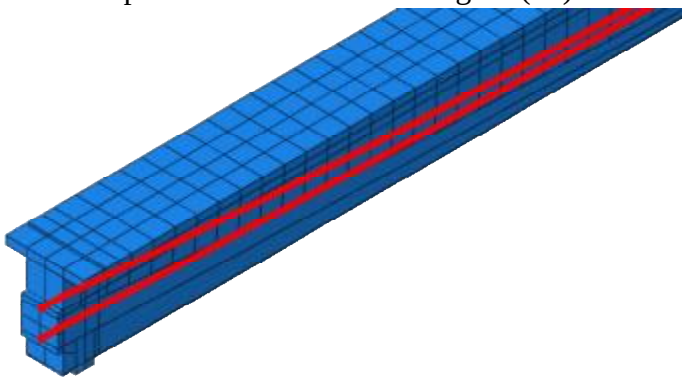

Figure (10) Surface to surface interaction between tendon and concrete

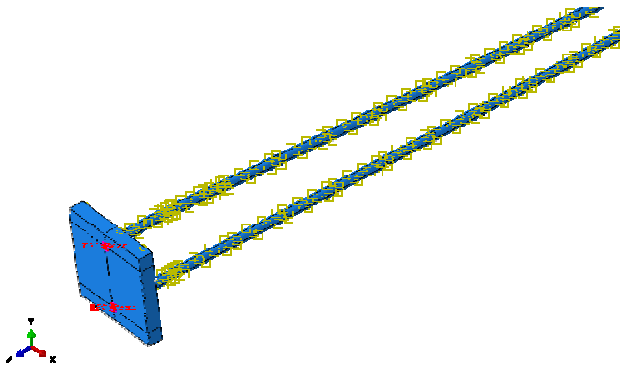

Figure (11) MPC beam Constraint between tendon end nodes and anchor plate

2.3 MESH CONFIGURATION

Figure (12) represents the finite element mesh of all beams where a more refined mesh was applied in the locations at which relatively high strain gradients are expected to take place. Modelling and mesh generation is developed using same techniques for all models, for concrete Part Mesh, (C3D8R) elements is used with approximate maximum mesh size of 100 mm. Figure (12) shows meshing of concrete beam in the model. Reinforcement mesh (T3D2) is used with approximate maximum element size of 50 mm. Figure (13) shows interior steel reinforcement bars in the models. For prestressing steel tendon Mesh, (C3D6R) elements is used with approximate maximum element size of 100 mm. the mesh technique is sweep meshing. Figure (14) shows meshing of prestressing tendons in the model. For FRP Bar Mesh, (T3D2) is used with approximate maximum size of 50 mm. Figure (15) shows FRP bars in the models. For Epoxy Mesh, (C3D8R) elements is used with approximate maximum element size of 100 mm as shown in figure (16)

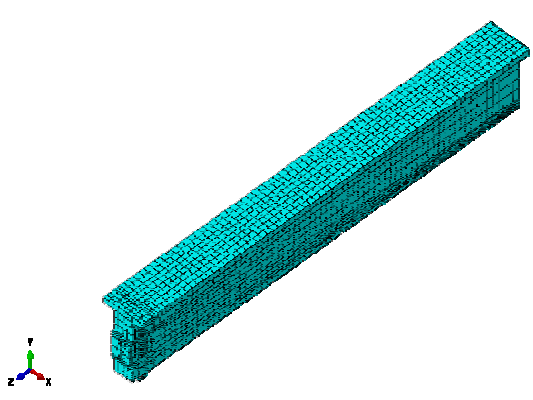

Figure (12) 3D Meshing of Concrete beam

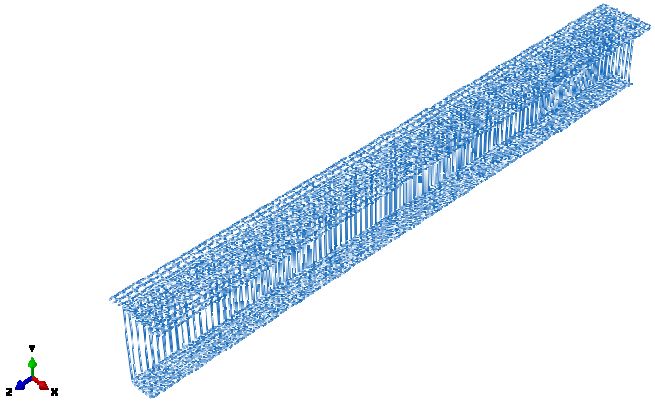

Figure (13) Interior steel reinforcement bars used in models

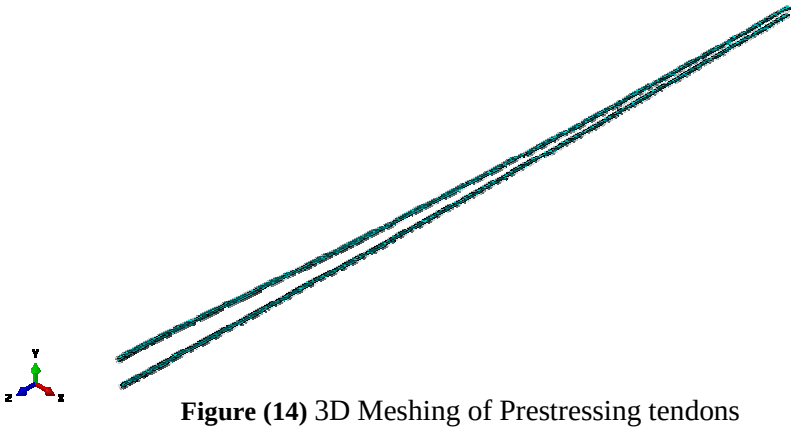

Figure (14) 3D Meshing of Prestressing tendons

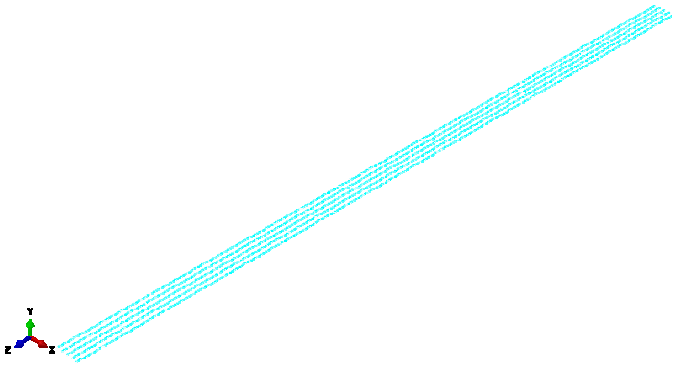

Figure (15) 3D Meshing of FRP bars

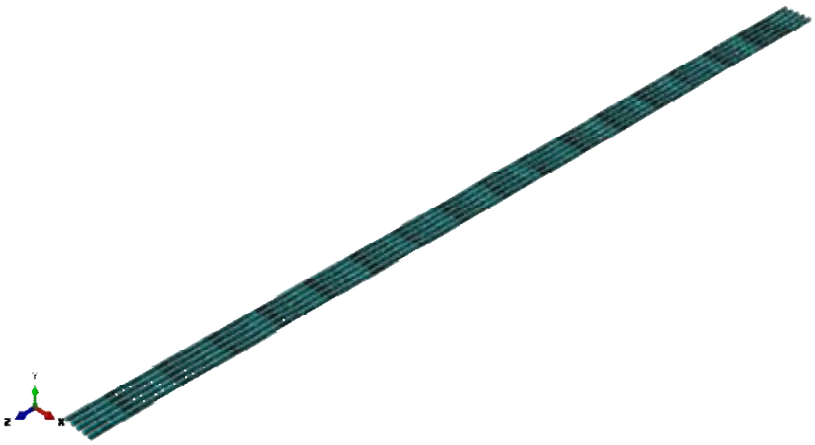

Figure (16) 3D Meshing of Epoxy Adhesive

2.4 LOADING APPLICATION AND BOUNDARY CONDITIONS

In this study three steps were created. Initial step that is always created by default in ABAQUS and two general analysis step. In this model the prestressing force applied as stress in tendon in the first step then the uniform load was applied as a load control in the second step. All the nodes in the centerline of support plate were restrained from the translation in X, and Y-directions (i.e. Hinged Support), similarly for those on the mid span which was restrained from the translation in Z-direction and the rotation about X and Y (i.e. UR1, UR2) (Symmetry boundary condition). Figure (17) illustrate the load application and restraints adopted in all the FE models.

2.5 FAILURE CRITERIA

In this study, the following assumptions are used to simulate and define the failure criteria of the developed models, adopted from the ACI 440.2R-08 code [15]:

1. Yielding of the steel in tension followed by concrete crushing failure when the strain in concrete in compression exceeds 0.003
2. FRP rupture failure is occurred when the strain in FRP exceeded ultimate strain in FRP (0.012).
3. FRP debonding of each beam is defined when Eq. (5) reaches (1) then the solution continuous then couldn't converge due to instability.

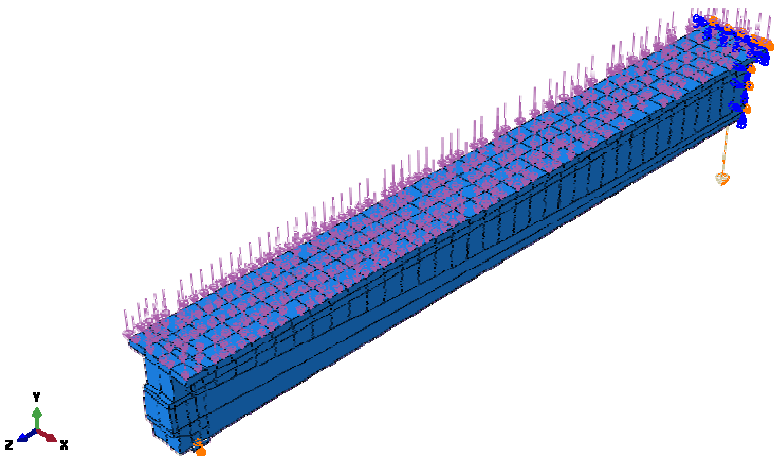

Figure (17) Loading technique in FE model

3. PARAMETRIC STUDY

A total of 20 FE models of strengthened Reinforced Concrete Post Tension simple beam with a span 29.6 m The details of strengthened posttension beams is found in figure (18). The finite element models are accounting for the effect of the percentage of prestressing steel (W_P). The specifications of the investigated beams are shown in table (1). "ABAQUS" finite element package is used to predict the behaviour of those beams to get the failure mode and the ultimate load.

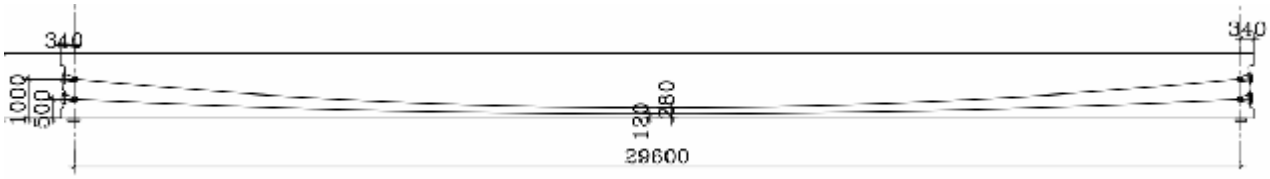

Figure (18) Details of strengthened posttension beam

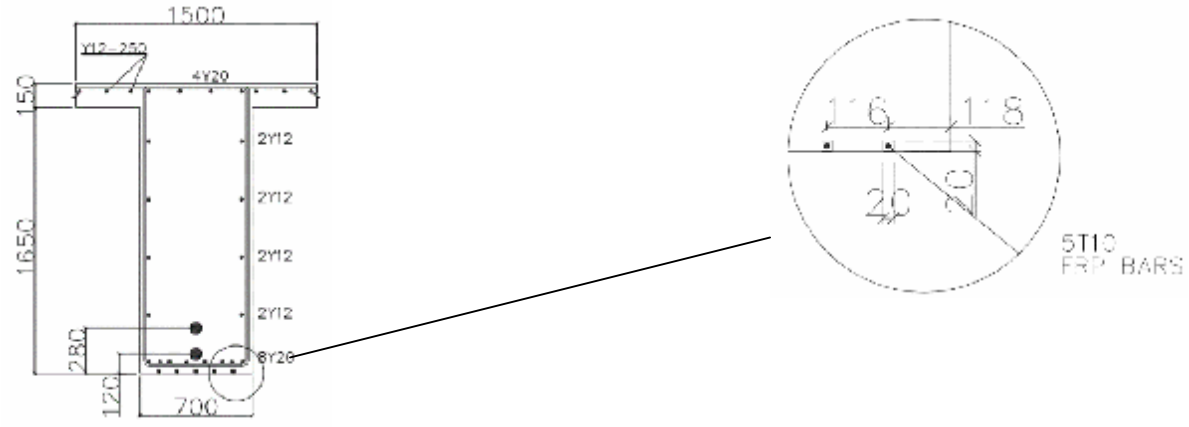

Group No.			Prestressing steel				Steel Reinforcement			FRP			
	beam label	Beam shape	Fc'(MPa)	Number and diameter of strands(mm)	Wp	F_{su}(MPa)	Number and diameter of bottom bars	Number and diameter of top bars	F_y(MPa)	NSM bar size(mm)	Number of bars	Embeded length(mm)	R = Afrp/Aps
Investigated Beams	B-ST28B-CB		40	28(15.24)	0.1	1860	8(20)	4(20)	420	-	-		-
	B-ST28B-5T10									10	5	28910	0.1
	B-ST28B-5T14									14	5		0.2
	B-ST28B-5T18									18	5		0.3
	B-ST28B-5T20									20	5		0.4
	B-ST56B-CB			56(15.24)	0.2					-	-		-
	B-ST56B-5T14									14	5	28910	0.1
	B-ST56B-5T20									20	5		0.2
	B-ST56B-5T24									24	5		0.3
	B-ST56B-5T28									28	5		0.4
	B-ST74B-CB			74(15.24)	0.3					-	-		-
	B-ST74B-5T16									16	5	28910	0.1
	B-ST74B-5T24									24	5		0.2
	B-ST74B-5T28									28	5		0.3
	B-ST74B-5T32									32	5		0.4
	B-ST94B-CB			94(15.24)	0.4					-	-		-
	B-ST94B-5T18									18	5	28910	0.1
	B-ST94B-5T26									26	5		0.2
	B-ST94B-5T32									32	5		0.3
	B-ST94B-5T36									36	5		0.4

Table (1) Details of Investigated beams

3.1 RESULTS OF PARAMETRIC STUDY

the load deflection curve is shown in figure (19). Figure (20) summarizes the increase in ultimate capacity with different values of Wp. Figure (21) illustrate the relation between the ultimate strain in the FRP (ε_{ufrp}) and the Ratio (A_{FRP}/A_{ps}) for different area prestressing ratio (W_P). table (2) summarize the results of the investigated beams.

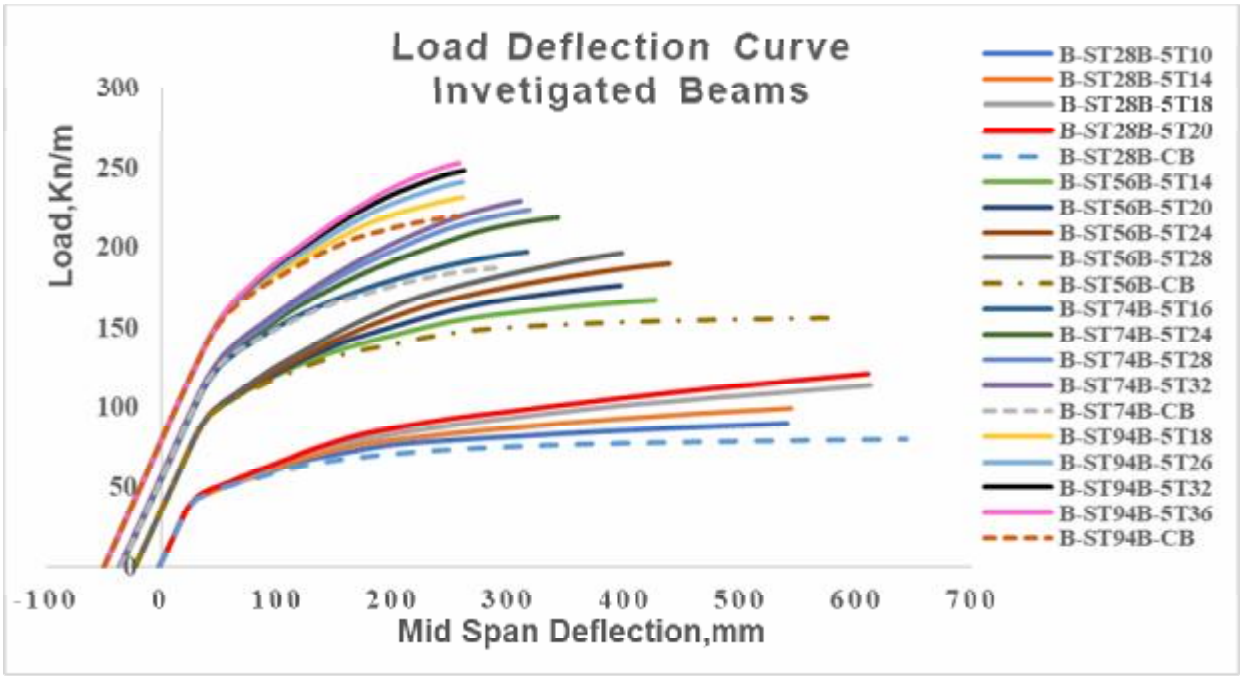

Figure (19) Load deflection curve for investigated beams

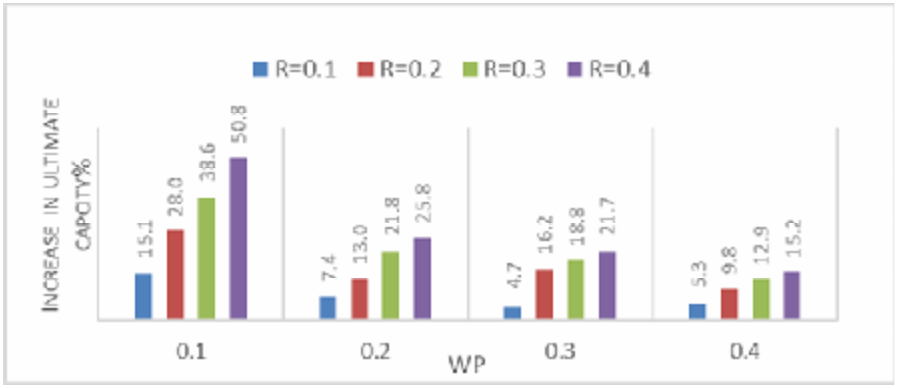

Figure (20) Summary of the increase in ultimate capacity%

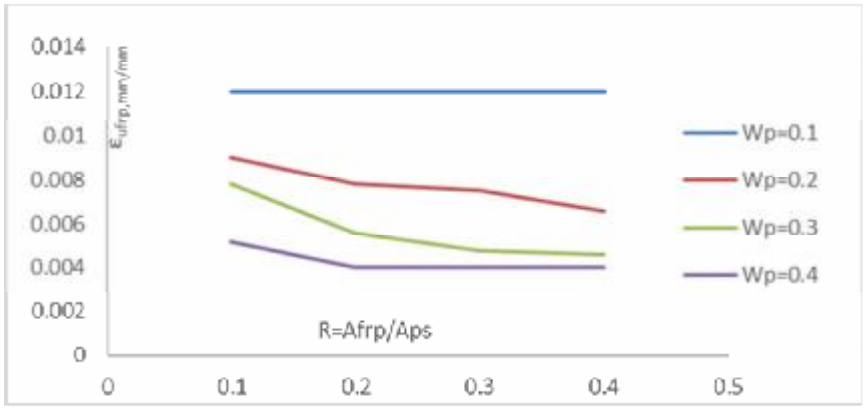

Figure (21) Summary of the ultimate strain in FRP bar

BEAM ID	Wp	R=A_{frp}/A_{ps}	P_U (KN/m)	δ_u (mm)	S=——— %	FAILURE MODE
B-ST28-CB	0.1	-	84.87	1189.12	-	PRES STEEL RUPTURE-CONCRETE CRUSHING
B-ST28-5T10		0.1	97.68	1026	15.1	FRP Debonding
B-ST28-5T14		0.2	108.6	875.58	28.0	FRP Rupture
B-ST28-5T18		0.3	117.63	680.43	38.6	FRP Rupture
B-ST28-5T20		0.4	127.98	726.3	50.8	FRP Rupture
B-ST56-CB	0.2	-	156.5	613.19	-	YIELDING OF PRES STEEL-CONCRETE CRUSHING
B-ST56-5T14		0.1	168.03	448.85	7.4	CONCRTE CRUSHING
B-ST56-5T20		0.2	176.79	419.09	13.0	CONCRTE CRUSHING
B-ST56-5T24		0.3	190.65	461.7	21.8	CONCRTE CRUSHING
B-ST56-5T28		0.4	196.86	406.69	25.8	CONCRTE CRUSHING
B-ST74-CB	0.3	-	188.4	329.1	-	YIELDING OF PRES STEEL-CONCRETE CRUSHING
B-ST74-5T16		0.1	197.23	351.18	4.7	CONCRTE CRUSHING
B-ST74-5T24		0.2	219	377.5	16.2	CONCRTE CRUSHING
B-ST74-5T28		0.3	223.88	353.97	18.8	CONCRTE CRUSHING
B-ST74-5T32		0.4	229.34	346.42	21.7	CONCRTE CRUSHING
B-ST94-CB	0.4	-	220.17	303.83	-	CONCRTE CRUSHING
B-ST94-5T18		0.1	231.76	309.5	5.3	CONCRTE CRUSHING
B-ST94-5T26		0.2	241.67	310.56	9.8	CONCRTE CRUSHING
B-ST94-5T32		0.3	248.6	311.48	12.9	CONCRTE CRUSHING
B-ST94-5T36		0.4	253.72	306.8	15.2	CONCRTE CRUSHING

Table (2) Summary of investigated beams results

4. ULTIMATE AND FAILURE MODE COMPARISON WITH [ACI440.2R-08]

A comparison is done for the ultimate load capacity & failure mode between finite element models and the empirical formula by ACI440.2R-08 as shown in table (3). The code implemented two failure modes (FRP Rupture or Debonding & concrete crushing) according to the effective strain in the FRP (ε_{fe}). For all strengthened beams, a fixed value of 0.7 was used for the bond-dependent coefficient of the FRP system (K_m) as there is no data to estimate it accurately. In order to get the ultimate moment capacity, the strength reduction factor $(\emptyset)$ is taken equal to 1.

The ACI 440 equations slightly underestimated the capacities of beams with 28 Strand with an average difference of 24.4% compared to the FEM capacities. Very reasonable predictions were obtained for beams with 56 Strand with an average difference of 4.2 % compared to the FEM capacities.

The ACI 440 equations slightly overestimated the capacities of beams with 74 Strand and 94 strand with an average difference of 10.8% & 16.3 respectively compared to the FEM capacities.

For beams with 28 strand, the calculations predicted a mode of failure of FRP debonding almost same as the FEM but for the beams with 56 strands the mode of failure predicted by the ACI 440 is FRP debonding while finite element models predicted a concrete crushing followed by FRP rupture. For beams with 74 & 94 strand, the calculations predicted a mode of failure of Concrete crushing as same as the finite element models.

Table (3) Comparison Between Ultimate Load Capacity For Investigated beams

	BEAM ID	Pu (KN/m) ABAQUS	Pu calc (KN/m) (ACI 440.2R-08)	Predicted Failure mode ABAQUS	Predicted Failure mode (ACI 440.2R-08)	——— %
G1	B-ST28-5T10	97.68	82.06	FRP Debonding	FRP Debonding	19.0
	B-ST28-5T14	108.6	87.40	FRP Rupture	FRP Debonding	24.3
	B-ST28-5T18	117.63	94.46	FRP Rupture	FRP Debonding	24.5
	B-ST28-5T20	127.98	98.62	FRP Rupture	FRP Debonding	29.8
	Average					24.4
	B-ST56-5T14	168.03	176.29	Concrete Crushing	FRP Debonding	-4.7
	B-ST56-5T20	176.79	186.70	Concrete Crushing	FRP Debonding	-5.3
	B-ST56-5T24	190.65	195.52	Concrete Crushing	FRP Debonding	-2.5
	B-ST56-5T28	196.86	205.74	Concrete Crushing	FRP Debonding	-4.3
	Average					-4.2
	B-ST74-5T16	197.23	230.14	Concrete Crushing	Concrete Crushing	-14.3
	B-ST74-5T24	219	241.52	Concrete Crushing	Concrete Crushing	-9.3
	B-ST74-5T28	223.88	247.93	Concrete Crushing	Concrete Crushing	-9.7
	B-ST74-5T32	229.34	254.59	Concrete Crushing	Concrete Crushing	-9.9
	Average					-10.8
	B-ST94-5T18	231.76	280.96	Concrete Crushing	Concrete Crushing	-17.5
	B-ST94-5T26	241.67	288.87	Concrete Crushing	Concrete Crushing	-16.3
	B-ST94-5T32	248.6	295.67	Concrete Crushing	Concrete Crushing	-15.9
	B-ST94-5T36	253.72	300.43	Concrete Crushing	Concrete Crushing	-15.5
					Average	-16.3

Table (4) Comparison Between Ultimate Load Capacity For Investigated beams

1. CONCLUSIONS

1. The use of near surface mounted CFRP reinforcement is feasible and effective for strengthening of posttension concrete beams.
2. For the beams investigated in parametric study group accounting for the effect of the percentage of prestressing steel w_p:
    a) Strengthening of beams with ratio of w_p=0.1 gave a significant increase in flexural capacity of about (15.1-50.8%) attributed to the fact that the beams sections tend to behave as under reinforced.
    b) Strengthening of section with ratio of w_p=0.4 gave a very small increase in capacity (3-15%) because the section is brittle and the governing failure is concrete crushing in compression and the ultimate strain in FRP bar is very small.
3. The ultimate strain in the FRP reduces as the Ratio of prestressing strands (W_P) in section increases indicating that the efficiency of strengthening is better under lower values of reinforcement ratios.
4. As the Ratio(A_{frp}/A_{ps}) increases in section the ultimate strain in the FRP decreases. The amount of strengthening doesn't have a significant effect on the stress in the prestressing strands. The decrease in the stresses in prestressing strands only reached 3% compared to the unstrengthened beams.
5. For the comparison made between finite element models and ACI 440.2R-0.8:
    a. The ACI 440 predicted a reasonable capacities of beams compared to the FE models.
    b. The predicted failure modes of ACI 440 slightly different between FEM models

REFERENCES

1. Hassan, T., and Rizkalla, S., (2002) "Flexural Strengthening of Prestressed Bridge Slabs with FRP Systems", PCI Journal, V. 47, No. 1, pp. 76-93.
2. Hassan, T., (2002) "Flexural Performance and Bond Characteristics of FRP Strengthening Techniques for Concrete Structures", PhD. Thesis, University of Manitoba, Winnipeg, Canada.
3. De Lorenzis L, Teng JG. Near-surface mounted FRP reinforcement: an emerging technique for strengthening structures. J Compos, Part B 2007;38:119–43.
4. Owen Arthur Rosenboom,(2006) "Behavior of FRP Repair/ Strengthening Systems for Prestressed Concrete"
5. Hawileh, R.A., Nonlinear finite element modeling of RC beams strengthened with NSM FRP rods. Construction and Building Materials, 2012. 27(1): p. 461-471.
6. Al-Mahmoud F, Castel A, François R, Tourneur C. Strengthening of RC members with near-surface mounted CFRP rods. Compos Struct 2009;91:138–47
7. Al-Mahmoud F, Castel A, François R, Tourneur C. Effect of surface preconditioning on bond of carbon fibre reinforced polymer rods to concrete.Cement& Concrete Compos 2007; 29:677–89
8. Mattock, A. H., "A Study of the Ultimate Moment of Resistance of Prestressed and Reinforced Concrete Beams, with Particular Reference to Bond Conditions," PhD Dissertation, University of London, 1955.
9. Thomas H.-K. Kang, Yu Huang, Myoungsu Shin, Ju Dong Lee, and Ah Sir Cho "Experimental and Numerical Assessment of Bonded and Unbonded Post-Tensioned Concrete Members" ACI Structural Journal,V.112,No.6, Nov.-Dec.2015 ,pp. 735-748
10. ABAQUS, "ABAQUS User's Manual, Volumes I to III," Pawtucket, RI, 2008.
11. Ellobody, E., and Bailey, C. G., 2008, "Testing and Modelling of Bonded and Unbonded Post-Tensioned Concrete Slabs in Fire," 5th International Conference on Structures in Fire, pp. 392-405.
12. Rezazadeh, M., S. Cholostiakow, R. Kotynia, and J. Barros, Exploring new NSM
13. reinforcements for the flexural strengthening of RC beams: Experimental and numerical research. Composite Structures, 2016. 141: p. 132-145.
14. Yasmeen Obaidat , Susanne Heyden, Ola Dahlblom , "The effect of CFRP and
15. CFRP/concrete interface models when modelling retrofitted RC beams with
16. FEM".Composite Structures,2009 p1391-1398
17. Hibbitt, Karlsson, and Sorensen, Inc. ABAQUS Theory manual, User manual and Example Manual, Version 6.7. Providence, RI; 2000
18. American Concrete Institute Technical Committee 440. Guide for the design and
19. construction of externally bonded FRP systems for strengthening concrete structures.
20. ACI 440.2R-02; 2008.